Available online at www.sciencedirect.com

ScienceDirect

Procedia CIRP 44 (2016) 298 – 303

www.elsevier.com/locate/procedia

6th CIRP Conference on Assembly Technologies and Systems (CATS)

Process Simulation and Automatic Path Planning of Adhesive Joining

Martin Svensson[a,*], Andreas Mark[a], Fredrik Edelvik[a], Jonas Kressin[a], Robert Bolin[a], Daniel Segerdahl[a], Johan S. Carlson[a], Per-Johan Wahlborg[b], Mathias Sundbäck[c]

[a] *Fraunhofer-Chalmers Research Centre for Industrial Mathematics, Chalmers Science Park, SE-412 88, Göteborg, Sweden*
[b] *Swerea IVF, Box 104, SE-431 22, Mölndal, Sweden*
[c] *Volvo Car Corporation, Volvo Car Sverige AB, SE-405 31, Göteborg, Sweden*

[*] Corresponding author. Tel.: +46-31-772-4245; *E-mail address:* martin.svensson@fcc.chalmers.se

Abstract

Adhesive joining is frequently used in the automotive industry. In the pursuit of reducing weight, adhesive joining is important due to the possibility of joining different types of materials. The process is often automatised in order to reduce cycle time. In this paper we aim to present a novel framework that includes detailed process simulation and automatic generation of collision free robot paths and in this way improve the quality of the joint and reduce both cycle time and processing time. To verify the simulations, the properties of the adhesive bead have been compared to experiments with good agreement.

Peer-review under responsibility of the organizing committee of the 6th CIRP Conference on Assembly Technologies and Systems (CATS)
Keywords: process simulation, rheology, VOF, volume of fluid, immersed boundary method, automatic path planning, computational fluid dynamics

1. Introduction

In 2015 the European Union has an emission target of 130 grams of CO_2 per kilometre for new cars that are registered in EU. On average, the cars produced in 2014 was well bellow this limit. However, in 2021 the target reduced to 95 $g\,CO_2\,/\,km$, which is a 23% reduction from the average emission levels from 2014. To meet this regulation, car manufacturers have to find different ways of reducing the fuel consumption. The use of light weight materials, separately or in combination with conventional steel structures, is an important step in this direction but by introducing new materials, new demands in the manufacturing process emerge.

Adhesive joining is a method which addresses the problems connected with multi-material combinations and weight reduction which is why many manufacturers are increasingly substituting welding methods in favour of adhesive joining. Since adhesive joining is a relatively new technique in mass production the process itself is not optimal. The processing time to design, plan and evaluate new adhesive features is long and there is a significant amount of material waste connected to it. To reduce processing time, off-line programming is used to plan the motion of the robotised adhesive dispenser but due to the complex characteristics of the adhesive the result is hard to predict and the station operator has to manually correct the motion to achieve satisfying results.

No previous attempts to simulate the adhesive dispensing process can be found in literature. There are however similarities with the sealing spray process where a few publication can be found [1,2]. In this paper we are proposing a method for combined process simulation and automatic path planning for adhesive joining applications. With this approach both the cycle time and processing time can be reduced and at the same time the quality of the joint, in a geometrical aspect, can be assured. In Section 2 we describe the process simulation, in Section 3 the automatic robot path planning and sequence optimization and in Section 4 how these are combined in the virtual product and production software Industrial Path Solutions (IPS).

2. Process simulation

The process simulation is based on numerically computing the flow of the adhesive as well as the surrounding air using IBOFlow, the in-house fluid flow solver at Fraunhofer-Chalmers Centre (FCC) [3]. Since the adhesive exhibits non-Newtonian properties, a Carreau-Yasuda rheology model is implemented. In order to validate the numerical framework, simulations where the adhesive is applied with different velocities, mass flows and at different heights are compared to experiments.

Peer-review under responsibility of the organizing committee of the 6th CIRP Conference on Assembly Technologies and Systems (CATS)
doi:10.1016/j.procir.2016.02.113

2.1. Numerical framework

The flow field is modelled by the incompressible Navier-Stokes equations

$$\nabla \cdot \bar{u} = 0$$
$$\rho_f \frac{\partial \bar{u}}{\partial t} + \rho_f \bar{u} \cdot \nabla \bar{u} = -\nabla p + \mu \nabla^2 \bar{u},$$

where $\bar{u}$ is the fluid velocity, ρ_f is the fluid density, p is the pressure and μ is the apparent viscosity defined as the ratio between shear stress and shear rate, $\mu = \frac{\sigma}{\dot{\gamma}}$. The finite volume method is used to solve the Navier-Stokes equations. The equations are solved in a segregated way and the SIMPLEC method derived in [4] is used to couple the pressure and the velocity fields. All variables are stored in a co-located arrangement and the pressure weighted flux interpolation proposed in [5] is used to suppress pressure oscillations. The two-phase flow is modelled with the Volume of Fluid (VOF) method, where the local property of the fluid is dependent on the volume fraction. The volume fraction is transported with the local velocity field. To keep the interface between the adhesive and the surrounding air sharp, a hybrid CICSAM convective scheme is adopted [6]. The Continuum Surface Force derived in [7] is used to model the surface tension. A Cartesian octree grid is used for the spatial discretisation of the fluid domain and dynamic refinements around moving objects and interfaces between phases in the flow are used.

Further, the immersed boundary method [8] is used to model the presence of moving objects, without the need of a body-fitted mesh. In the method, the fluid velocity is set to the local velocity of the object with an immersed boundary condition. To set this boundary condition, a cell type is assigned to each cell in the fluid domain. The cells are marked as fluid cells, extrapolation cells, internal cells or mirroring cells depending on the position relative to the immersed boundary. The velocity in the internal cells is set to the velocity of the immersed object with a Dirichlet boundary condition. The extrapolation and mirroring cells are used to construct implicit boundary conditions that are added to the operator for the momentum equations. This results in a fictitious fluid velocity field inside the immersed object. Mass conservation is ensured by excluding the fictitious velocity field in the discretised continuity equation. A thorough description of the method and an extensive validation can be found in [8].

Adhesive is injected to the domain through source cells located at the position of the orifice of the dispenser. The fluid velocity in these cells corresponds to the mass flow obtained by

$$\dot{m} = \rho v_{robot} \left(\frac{\Phi_{nom}}{2} \right)^2,$$

where ρ is the density of the adhesive, v_{robot} is the velocity of the dispenser and Φ_{nom} is the nominal diameter of the bead.

2.2. Rheology

The apparent viscosity of the adhesive is modelled according to the Carreau-Yasuda model [9],

$$\mu = (\mu_0 - \mu_\infty) \left(1.0 + (\lambda \dot{\gamma})^2 \right)^{0.5(N-1)} + \mu_\infty,$$

where the apparent viscosity, μ, is dependent on the local shear rate, $\dot{\gamma}$, λ and N are material constants derived from experiments, see Table 1 and μ_0 and μ_∞ are the zero-shear-rate viscosity and the infinite-shear-rate viscosity which represents the upper and lower Newtonian plateaus defined as

$$\lim_{\dot{\gamma} \to 0} \frac{\sigma_{xy}}{\dot{\gamma}_{xy}} = \mu_0$$

and

$$\lim_{\dot{\gamma} \to \infty} \frac{\sigma_{xy}}{\dot{\gamma}_{xy}} = \mu_\infty.$$

Table 1. Carreau-Yasuda parameters for M91 rubber adhesive

Parameter	Value (t)	Unit (t)
Zero-shear-rate viscosity, μ_0	130000	$Pa \cdot s$
Infinite-shear-rate, μ_∞	60	$Pa \cdot s$
Carreau time constant, λ	1000	s
Power law index, N	0.3	-

The rheology model is shown in Figure 1 together with experimental data of the M91 structural rubber adhesive used extensively at Volvo Car Corporation from cone-plate rheometer measurements performed at Swerea IVF and parallel plates and capillary rheometer measurements from [10].

2.3. Validation

The numerical framework and rheology model are validated by simulating three different bead set-ups with different properties, see Table 2.

Table 2. Set-up variations for different beads.

Bead set-up	Nominal diameter (mm)	Application speed (mm/s)	Application height (mm)
Bead 1	2.5	150	2.5
Bead 2	3.5	300	3.5
Bead 3	5	300	5

Simulations are then compared to experimental data where the three different set-ups are used to apply adhesive to a sheet metal plate with length 200 mm using a SCA dispenser, model

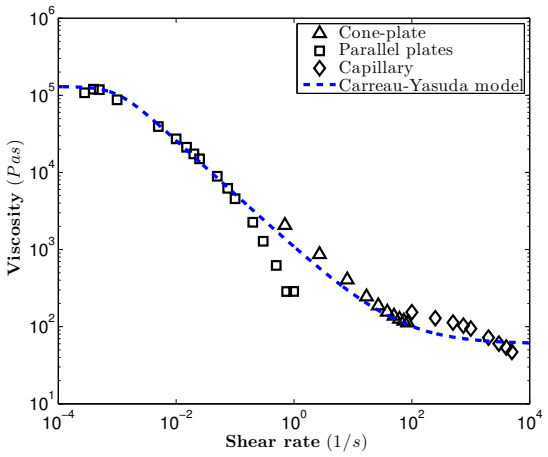

Figure 1. □, △ and ◊ indicates values from cone-plate, parallel plates and capillary plate, rheometer measurements respectively for M91 rubber adhesive. The –– line shows the Carreau-Yasuda model that is implemented in IBOFlow.

AK403 with a nozzle diameter of 2 *mm* and ASC5000 control system, mounted to an ABB robot, model IRB 6600-175/2.8 type B, located at Swerea IVF. The beads are scanned using a GOM Athos III tripplescan. The average height and width of the cross section of three different beads are then compared to simulations with the same set-up. It should be mentioned that the nominal plate used for the simulation and the scanned plate differ approximately 1 *mm* in vertical direction. This potentially affects the measured bead geometry since the dispenser height is varying both along the beads and between different beads with the same set-up. Due to these variations in the experimental set-up, additional simulations where carried out with a 50% increased dispenser height to get an estimate of the sensitivity to this process parameter. The height and width at the beginning and at the end of scanned bead are displayed individually. The results can be seen in Figure 2.

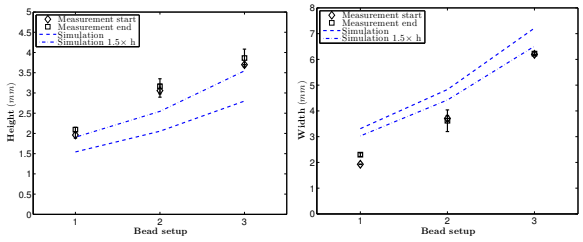

Figure 2. Comparison of height (left) and width (right) between simulation and experiments for three different bead set-ups.

For bead set-up 3, fluid buckling occurred for at least one bead. Fluid buckling occurs when the momentum of the flow cannot overcome the internal resistance within the fluid. A similar mechanism to that of Euler buckling for an axially loaded column. In this case only data from one cross section is used. The simulation height differs from the experimental data by 6%, 18% and 4% for bead set-up 1, 2 and 3 respectively, whereas the width differs by 43%, 21% and 5%. The reason for the relatively large difference in width for bead set-up 1 can be explained by the fact that the simulation is over predicting the impact energy for short distances between nozzle and substrate, since the material injection is located exactly at the nozzle orifice. Since the momentum is large, the viscous forces are not strong enough to sustain the round shape of the bead. Instead the material is pushed outwards and the bead width increases.

3. Automatic robot path planning and sequence optimization

This section describes a method for automatic programming of a robotised adhesive station. The method is based upon the work in [2], and consists of the following major steps:

1. creating task definitions by finding appropriate nozzle orientations along each adhesive curve,
2. finding for each task a set of feasible motions allowing the robot to follow the adhesive curves
3. sequence optimization and motion planning in order to select one solution for each bead and connect them by efficient motions and to minimize cycle time.

These three steps are briefly described on the following subsections.

3.1. Task definition and process constraints

The purpose of this step is to create an oriented curve defined by a sequence of target frames. Assuming that each task is originally described by a curve defining the centre of the adhesive bead, the geometry around the curve can be locally analysed in order to calculate a task definition, D, such that

- it deviates no more than a specified threshold (default 3 *mm*) from the original curve
- it contains a minimum number of frames
- its x-axis is aligned with the curve tangent
- its z-axis points in a desired direction of application
- the orientation of successive frames differs no more than a specified threshold (default 20°)
- between two successive frames, linear interpolation is used to define intermediate frames.

Under ideal conditions, the nozzle's TCP should follow the task definition D with a certain velocity, but in many cases this would lead to numerous conflicts with surrounding geometry, kinematic singularities or joint limits. By deviating somewhat from the ideal nozzle orientation defined by D, the creation of collision-free, smooth robot motions is facilitated. The maximal deviation is expressed in terms of process constraints here limits on tilt, drag and spin angles around x-, y- and z-axis, respectively. See [2] for further details.

3.2. Task planning

In the task planning step, our path planner searches for collision-free, smooth, and low cost robot paths along the adhesive beads [2]. The cost associated with a motion is a weighted sum of penalties for execution time, joint motion, deviation from task definitions, and small clearance. See also [11,12]. In this setting, each adhesive task can be performed in many ways

- some beads can be reached by more than one robot, from several slider positions (if sliders are present), and using multiple inverse configurations. Each bead can also be traversed in two directions. For each possible discrete configuration (choice of robot, inverse configuration and bead direction), the path planner tries to generate a low cost solution in the continuous variables (tilt, drag and spin deviations and slider position).

3.3. Sequence optimization

The final step decides in which order and with what alternative configuration the robot should lay down the adhesive, as well as how to move between the tasks in order to minimize cycle time. This Grouped Travelling Salesman Problem (GTSP), where each node has alternatives, is a generalization of the classical TSP. Due to the inherent computational complexity of automatic path planning, we utilize a lazy method minimizing the number of calls to the path planner. Instead of calculating all entries in the full cost tensor m_{ijkl} between alternative j and l of curve i and k, respectively, and then applying a GTSP solver to find the optimal solution, we initialize the cost tensor by trivial linear motions (i.e., ignoring all obstacles) between all pairs of alternatives. Then we incrementally update the cost tensor by iteratively finding the best sequence, performing path planning where needed, and updating the cost tensor. In this way, the optimal solution can be found with minimal calls to the path planner. The sequence optimization is illustrated on a schematic case in Figure 3.

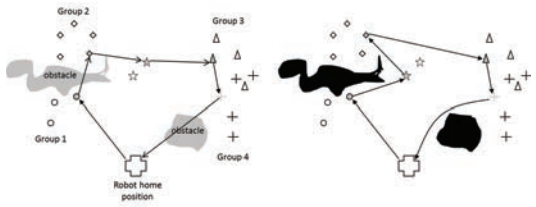

Figure 3. Lazy evaluation of a four group generalized TSP problem with obstacles. Left figure shows the optimal routing before path planning. Right figure shows the re-routing after a number of iteration considering collisions with the obstacles.

4. Methodology

The proposed method combines process simulations with automatic path planning. In this way, it is possible to complete major part of the product preparation off-line and only use a minimum of physical testing. Each path can be evaluated with regard to bead geometry directly and corrected before the program is exported to the robot. The path planning algorithm described in 3 and the fluid flow solver described in Section 2.1 are implemented as modules in IPS. As input to the modules in IPS the user provides a robot cell, a triangulated surface of the substrate, a geometrical curve of the location of the desired adhesive bead and process properties of the dispense equipment. The algorithm will use this information to create a collision free path. The generated path is then imported, together with substrate geometry and a set of simulation parameters, to the numerical simulation of the flow field. The work flow of can be seen in Figure 4.

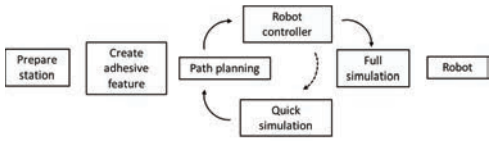

Figure 4. Work flow of the proposed method.

5. Case

To verify the work flow, the proposed method is used to plan and simulate the complete process of an adhesive application on a set-up similar to an industrial case and compare the result with experimental data. The geometry is an inner body side provided by Volvo Car Corporation. The robot and dispenser system is the same as for the sheet metal plate validations from Section 2.3 and can be seen in Figure 5. The nominal bead diameter is 2.5 *mm*, the dispenser velocity is 100 mm/s and the height is 3.5 *mm*.

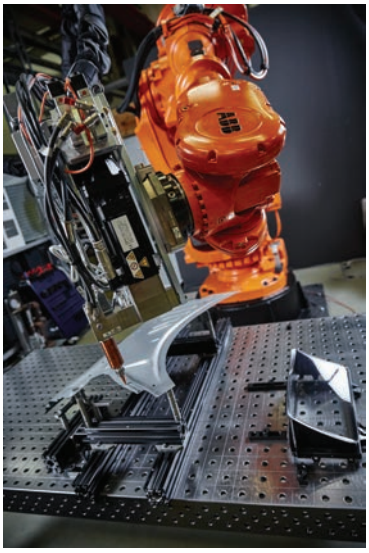

Figure 5. The robot cell at Swerea IVF applying adhesive onto the case test geometry.

IPS does not include information about the robot controller so in order to make fair comparison between experiment and simulations, the path created in IPS is exported to ABB Robot Studio, adjusted using the controller and then imported back to IPS. In this way both the experimental- and the numerical set-up have the same path to follow, assuming that the robot does not deviate from the path due to dynamical effects. In this demonstration case the optimisation loop, seen in Figure 4, is not performed. Instead the geometry of the simulated bead is compared directly with the experimental bead.

5.1. Robotics and automatic path planning

There are ten curves on the demo case which are converted to parametrized line segments. The robot path is allowed to deviate 3 *mm* from these lines to create smooth robot motions. The maximum distance from the curve is set to 5 *mm* and for the inter path motion the minimum clearance from surrounding ge-

ometries is constrained not to fall below 10 *mm*. IPS generates a number of possible ways to follow the each bead individually and then finds a collision free robot motion between all of the beads that is optimized with respect to cycle time. The virtual demonstration cell can be seen in the IPS software in Figure 6.

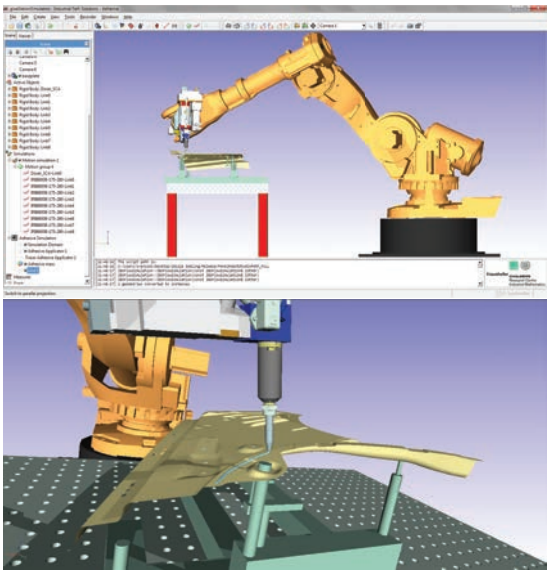

Figure 6. Snapshots of the adhesive cell in the IPS software. The robot is applying adhesive onto the inner car body side used as demo case.

On a single work station, the path planning took 5 minutes and 10 seconds while the sequence and inter path planner needed 12 seconds to find an acceptable solution. This resulted in a total cycle time of 23 seconds for the demo case.

5.2. Results

Even though the selected demo case consists of ten adhesive beads, only the process simulation result from one of them is presented here. The reason for this is that the major part of them are straight lines which are trivial to perform. Instead, a bead containing curvatures and stamped sections is chosen to validate the process simulation. The simulated bead and case geometry can be seen together with the computational domain in Figure 7. The domain is refined dynamically around the bead which greatly reduces the number of cells without compromising with the accuracy. The smallest cubic cell is 0.625 *mm* and the Courant-Friedrichs-Lewy condition, defined as the maximum velocity multiplied by the ratio between the time step and the cell size at the location of the maximum velocity, is kept at approximately 0.1. The material is the M91 rubber adhesive characterised in Section 2.2.

The result from the simulation is shown in Figures 8 and 9 together with the scanned experimental bead. As can be seen in Figure 8, the position of the simulated bead (blue) corresponds very well to the experimental bead (grey). In order to study the shape of the beads more closely, four cross sections are chosen to represent regions with different characteristics. These are magnified and shown in the right part of the figure. It should be mentioned that in this part of the figure, the simulated bead is translated approximately 10 *mm* in order to see the shape of the

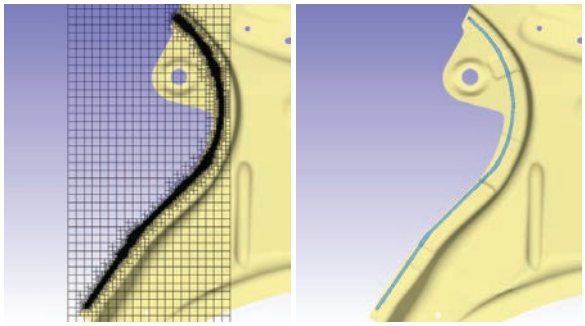

Figure 7. The simulated adhesive bead with adaptive grid refinements.

beads more clearly. Firstly, there are regions where the robot has to perform more complicated motions in order to follow the prescribed path within the tolerance. The dispenser speed is not necessarily constant here since the criteria of position is overruling the criteria of dispenser speed. This typically occurs where the geometry is stamped so that the normal of the object suddenly changes significantly. Such a region is most prominent at Cross section 1 where there is an upward step in the geometry. The shape of the simulated bead corresponds well to the experimental one even though the width, see Figure 9, is somewhat under predicted. The reason for this might be due to vertical disturbances of the robot that was observed in regions with strong deceleration. Secondly, there are regions with constant dispenser speed and simple robot joint movements. Cross section 2 is an example of such a region. In this region the simulation corresponds very well with experimental data. Finally, at Cross section 3 the path is curved with respect to the vertical axis and at Cross section 4 the path is experiencing a downward step. At both of these section the experimental bead is experiencing fluid buckling. Even though this feature is not present in the simulations, the height and width of the bead at these regions correspond well with experiments.

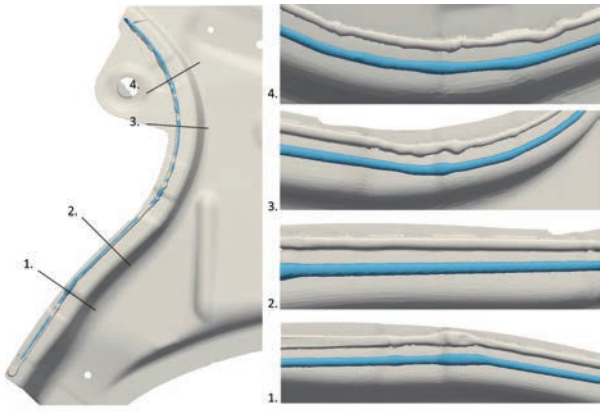

Figure 8. Comparison between the scanned experimental bead (grey) and a simulated adhesive bead (blue). Four sections of particular interest are magnified.

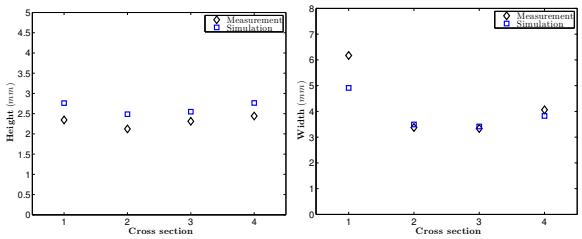

Figure 9. The height (left) and width (right) of the scanned experimental bead compare with the simulated adhesive bead at cross sections 1-4. The height of the simulated bead at cross sections 1-4 differs from the experimental data with 18%, 17%, 10% and 13% whereas the width differs with 20%, 3%, 2% and 6%.

6. Conclusions

The prosed framework is capable of planning collision free, sequence optimized paths for adhesive application which are directly exportable to a robot-carried dispenser system. The automatic path planning algorithm in combination with process simulation of adhesive dispensing results is a powerful tool where deviation from an optimal bead geometry directly can be corrected. Collision free paths of the ten beads included in the demo case is generated in approximately five minutes and the complete sequence takes an additional 12 seconds on a single work station. Simulation of the 440 *mm* long adhesive bead used in the demo case is simulated, again on a single work station, within 10 hours. Results from the process simulations corresponds well with experimental data except for beads with low dispenser height where the height is under predicted and the width is over predicted. This is an effect of high inertia in the nozzle orifice in relation viscous forces in the fluid. Furthermore, fluid buckling did not occur in the simulation even though it was observed in experiments. To be able to capture the fluid buckling phenomena correctly in the simulations, a finer grid and a smaller time step than what is considered feasible for industrial purposes is needed. Finally and perhaps most importantly, problematic regions could be identified in the simulation and corrected without having to perform physical testing. In combination with automatic path planning and sequence optimization, this makes it possible to reduce both cycle time and processing time and at the same time ensure the quality of the adhesive bead.

Acknowledgements

This work was supported in part by the Swedish Governmental Agency for Innovation Systems, VINNOVA, through the FFI Sustainable Production Technology program, and in part by the Sustainable Production Initiative and the Production Area of Advance at Chalmers. The test geometries and experimental data were provided by Volvo Car Corporation and Swerea IVF respectively. The support is gratefully acknowledged.

References

[1] Rundqvist, R., Mark, A., Edelvik, F., Carlson, J.S.. Modeling and simulation of sealing spray application using smoothed particle hydrodynamics. Fluid Dynamics & Materials Processing 2011;7(3):259–278.
[2] Mark, A., Bohlin, R., Segerdahl, D., Edelvik, F., Carlson, J.S.. Optimisation of robotised sealing stations in paint shops by process simulation and automatic path planning. International Journal of Manufacturing Research 2014;9(1):4–26.
[3] Mark, A.. The mirroring immersed boundary method. Ph.D. thesis; Chalmes University Of Technology, Göteborg; 2008.
[4] Van Doormal, J., Raithby, G.. Enhancement of the simple method for predicting incompressible flows. Numerical Heat Transfer 1984;7:147–163.
[5] Rhie, C., Chow, W.. Numerical study of the turbulent flow past an airfoil with trailing edge separation. AIAA J1 1983;21:1527–1532.
[6] Ubbink, O.. Numerical prediction of two fluid systems with sharp interfaces. 1997. PhD. Thesis, Department of Mechanical Engineering, Imperial College of Science, London, United Kingdom.
[7] Brackbill, J., Kothe, D., Zemach, C.. A continuum method for modeling surface tension. J Comp Phys 1992;100:335–354.
[8] Mark, A., Rundqvist, R., Edelvik, F.. Comparison between different immersed boundary conditions for simulation of complex fluid flows. Fluid Dynamics & Materials Processing 2011;7(3).
[9] Yasuda, K.. Investigation of the analogies between viscometric and linear viscoelastic properties of polystyrene fluids. Ph.D. thesis; 1979.
[10] Eklund, J.. Rheological characterization of adhesives for use in modeling of adhesive application in simulation software ips. Master's thesis; Chalmers University of Technology; 2015.